Modeling the Thermal Dynamics inside a Ceria-Coated Gasoline Particulate Filter

Harikesh Arunachalam, *Student Member, IEEE*, Gabriele Pozzato, Mark A. Hoffman, and Simona Onori*, *Senior Member, IEEE*

***Abstract*— This work presents the first-ever control oriented model to predict the thermal dynamics inside a ceria-coated Gasoline Particulate Filter (GPF). By incorporating catalytic reaction kinetics in addition to the carbon to CO_2 oxidation reactions, the proposed model predicts the internal GPF temperature during nominal operation and regeneration events. The model utilizes the GPF inlet exhaust gas temperature to predict the internal GPF temperature. Parameter identification and model validation are performed using data obtained from experiments with a ceria-coated GPF installed on a vehicle using a direct injection engine operated in a chassis dynamometer laboratory. It is demonstrated in this work that the model predicts ceria-coated GPF thermal dynamics for different initial soot loadings and engine operating conditions within a root mean square (RMS) error of 5%.**

Nomenclature

$A_{C,1}$	Pre-exponential factor for the endothermic ceria reactions, $[1/s]$
$A_{C,2}$	Pre-exponential factor for the exothermic ceria reaction, $[1/s]$
A_T	Pre-exponential factor for the oxygen-initiated carbon oxidation reactions, $[1/s]$
$C_{p,GPF}$	Heat capacity of the GPF, $[J/(kgK)]$
$C_{p,g}$	Heat capacity of the exhaust gas, $[J/(kgK)]$
$E_a^{C,1}$	Endothermic catalytic reactions activation energy, $[J/mol]$
$E_a^{C,2}$	Exothermic catalytic reaction activation energy, $[J/mol]$
E_a^T	Exothermic carbon oxidation reactions activation energy, $[J/mol]$
$\Delta H_{C,1}$	Endothermic catalytic reactions enthalpy, $[J/mol]$
$\Delta H_{C,2}$	Exothermic catalytic reaction enthalpy, $[J/mol]$
ΔH_T	Exothermic carbon oxidation reactions enthalpy, $[J/mol]$
λ	Air/fuel ratio, $[-]$
m_C	Mass of carbonaceous soot, $[kg]$
M_C	Carbon molar mass, $[kg/mol]$
$\dot{m}_g$	Exhaust gas mass flow rate, $[kg/s]$
m_{O_2}	Mass of oxygen, $[kg]$
M_{O_2}	Oxygen molar mass, $[kg/mol]$
n_{tot}	Combustion reaction total product moles, $[mol]$
R	Ideal gas constant, $[J/(molK)]$
$R_{C,1}$	Endothermic ceria reaction rate, $[mol/s]$
$R_{C,2}$	Exothermic ceria reaction rate, $[mol/s]$
R_T	Oxygen-initiated carbon oxidation reaction rate, $[mol/s]$
ρ_{GPF}	Filter density, $[kg/m^3]$
ρ_{O_2}	Density of oxygen, $[kg/m^3]$
ρ_{soot}	Initial soot loading, $[g/l]$
T_{inlet}	Measured temperature at the GPF inlet, $[K]$
T_{mid}	Measured temperature at the mid-location of the GPF, $[K]$
T_{mod}	Model-predicted temperature at the mid-location of the GPF, $[K]$
V_{GPF}	Total volume of Cordierite in the GPF, $[m^3]$
V_{trap}	Filter trapping volume, $[m^3]$
X_{CeO_2}	Volume fraction of ceria, $[-]$
X_{O_2}	Volume fraction of oxygen, $[-]$

[1]Department of Automotive Engineering, International Center for Automotive Research, Clemson University, Greenville, South Carolina 29607 {harunac,gpozzat,mhoffm4,sonori}@clemson.edu

* corresponding author

I. Introduction

In recent years, the challenges associated with vehicular exhaust emissions have gained increasing prominence due to the imposition of stringent regulations for reducing greenhouse gases and particulate matter [1]. To meet current and future regulation targets, different engine technologies have been developed. Some of these new technologies are: (a) vehicle electrification [2], (b) gasoline direct injection (GDI) engines [3], (c) variable valve timing [4], (d) advanced exhaust gas recirculation [5], (e) waste heat recovery from Rankine cycle [6], and (f) selective catalytic reduction for NO_x [7].

GDI engines have become a preferred technology for automotive manufacturers to increase fuel economy while reducing greenhouse gas emissions [8]–[10]. However, the main drawback of this technology could be partial mixing of fuel and air for some combustion systems under certain operating modes. As a result of partial mixing, for certain systems under certain operating conditions, ultra-fine toxic

particulate matter could be released into the atmosphere, which may lead to environmental hazards and health diseases [11]–[13]. The Euro VI regulations emphasize the need for tighter enforcement of current particulate matter regulations from GDI engines. In this regard, the European Union is tightening the particulate number standard for GDI engines from 6×10^{12} particles/km to 6×10^{11} particles/km in the year 2017 [4].

Among the different strategies being pursued to effectively reduce these hazardous particulate emissions, devices such as Gasoline Particulate Filters (GPFs) are considered by original equipment manufacturers as the most practically adoptable and expediently deployed solution [14], [15]. GPFs consist of a monolithic structure with a bundle of axially parallel channels. These channels are alternatively plugged at each end and force the exhaust gas to flow through the porous walls. During this process, particulate matter is trapped in the GPF pores and separated from the exhaust gas constituents [16]. During vehicle operation, this particulate matter accumulates over time inside the GPF. Oxidation at elevated temperatures converts the trapped carbonaceous matter into CO and CO_2 gases, and reduces the trapped soot mass and associated back pressure in the filter [17].

Mitigation of exhaust gas emissions has already been pursued on diesel engines through diesel particulate filters (DPFs), and results have shown substantial reduction in soot mass and number at the tailpipe [18]–[20]. The characteristic behavior of DPFs, such as filtration efficiency and pressure drop, depend on parameters such as substrate cell density, porosity, pore size, wall thickness, and washcoat material [21]. However, gasoline exhaust properties and soot particle characteristic diameters are very different from those of diesel engines [3], making it inaccurate to apply DPF technology directly to GDI engines without making adjustments to the filter parameters.

A wealth of literature was published on DPFs, which focused on experimental investigations and mathematical model development ranging from lumped parameter strategies [22] to comprehensive models that incorporate the soot microstructure [23]. By contrast, very little information has been made available on the mathematical modeling of GPF physical dynamics. Nicolin $et.\ al.$ [24] and Boger $et.\ al.$ [25] proposed reduced order models to investigate the thermal dynamics in an uncoated GPF. Soot oxidation dynamics were modeled by studying regeneration events inside the GPF. Opitz $et.\ al.$ [16] proposed a single channel model and conducted experimental and simulation studies to investigate the cold start behavior of a GPF. Liu $et.\ al.$ [26] developed a mathematical model to determine the backpressure and filtration efficiency in metallic fibrous GPFs, and utilize this information to optimize design characteristics such as filtration area, filter thickness, and minimum filter media volume. A high fidelity 2-D physics-based model was developed to characterize mass, energy, and momentum transport of the exhaust gas inside an uncoated and clean GPF [27].

One challenge in characterizing GPF transport dynamics is that the filtration and regeneration mechanisms which continuously oxidize loaded soot have not been clearly understood. An approach to address this challenge is to install temperature sensors at different locations inside the GPF. However, the high costs involved with installation, data acquisition, monitoring, and maintenance makes this an infeasible option for real-world applications. A more viable approach is to develop mathematical models that incorporate the mass and heat transfer dynamics to predict the internal temperature dynamics in a GPF.

Recent advancements in GPF design have led to the development of $washcoated$ filters in which the monolithic structure is coated with inorganic oxides or precious metals such as platinum [28], [29]. Through experiments, such devices have been shown to reduce NO_x emissions by nearly 10% relative to uncoated GPFs [29]. Washcoated GPFs have also demonstrated enhanced soot oxidation with respect to their uncoated counterparts due to their inherent oxygen storage capability [11], [30]. In addition, Lambert $et.\ al.$ [31] specify that the initial filtration efficiency of an uncoated GPF can be improved by 20-30$\%$ by adding a catalyst washcoat. Washcoated GPFs are expected to be increasingly adopted in the future due to their ability to provide the following enhancements with respect to uncoated GPFs: (a) enhanced oxidation and reduction of gaseous emissions which slip through the three-way catalyst (TWC), (b) reduced pressure drop, and (c) improved particulate number filtration efficiency [32].

Compared to uncoated GPFs, washcoated GPFs have demonstrated the ability to perform regeneration more efficiently at lower temperatures [33]. They have also been experimentally observed to enhance soot oxidation, leading to hotter temperatures than their uncoated counterparts [3]. These factors elucidate the need for a mathematical approach that allows optimal utilization of washcoated GPFs by: (a) determining the internal GPF temperature variation during regeneration, and (b) accurately quantifying the amount of soot oxidized during regeneration. The successful accomplishment of objective (a) will facilitate GPF operation within safe limits of temperature and prolong its useful life. Achieving objective (b) in addition to objective (a) will enable control of the necessary regeneration duration. Thus far, washcoated GPF models which characterize the thermal and soot oxidation dynamics are lacking in the published literature.

For the very first time, we propose a lumped parameter model to characterize the thermal dynamics in a ceria-coated GPF. In addition to oxygen-initiated soot oxidation reactions, this model incorporates ceria-influenced catalytic reactions to determine the overall exothermic heat during regeneration events. The formulation of the reaction rate equations not only allows the prediction of internal temperature, but also the amount of soot oxidized as a function of time. An additional benefit of the proposed model is understanding how the active ceria sites are generated and consumed within the GPF. A similar approach can be implemented for any catalytic coating material. As a result, the amount of soot oxidized can be quantified for each type of washcoat material

used in the GPF. This information can be very useful for coated-GPF design purposes.

This paper is structured as follows: Section II presents the lumped parameter model, reaction rates, thermal balance equation, variation of carbon soot mass, and the mass balance of available catalytic ceria sites during the operation of the coated GPF. Section III presents the model parameter identification approach using two different experimental data sets. Section IV validates the performance of the lumped parameter model using a third experimental data set with an initial soot loading concentration and operating conditions that are different from the identification data sets. Section V summarizes the contributions of this work and the direction of future research to enhance model predictiveness.

II. Dynamic Transport Model of a Ceria-Coated GPF

In this section, a lumped parameter model is presented to characterize the thermal dynamics in a coated GPF. The washcoat material used in the GPF is composed of cerium (Ce), a catalytic element that is capable of enhancing soot oxidation reactions inside the GPF. First, reaction rate expressions are formulated for all regeneration reactions. Using this information, the amount of heat released during the regeneration event is quantified. By combining exhaust gas convection heat transport and the conduction heat transfer through the thermal inertia of the cordierite material, the thermal dynamic equation is developed. The reaction rate equations are also used to determine the soot mass dynamics and the formation-consumption of active ceria sites. Accurate information regarding the thermal dynamics inside a GPF is important since GPF operation beyond certain critical internal temperatures can lead to ceramic substrate fracture and/or damage to the washcoat. On the other hand, information about the soot oxidation dynamics can help prevent filter overloading and elevated back pressure.

The exothermic, oxygen-initiated, soot oxidation reactions, introduced in [24], are:

$$\left.\begin{array}{l} C + O_2 \rightarrow CO_2 \\ C + 0.5O_2 \rightarrow CO \end{array}\right\} \textbf{Exothermic} \tag{1}$$

To define the reaction rate expression for each of the above exothermic reactions, the extent of partial oxidation that produces CO, and the extent of complete oxidation that produces CO_2 must be explicitly known. It is challenging to quantify these oxidation pathways individually due to the difficulty in measuring the amount of CO produced as an intermediate step towards ultimate CO_2 production at the GPF outlet. As a result, a unified reaction rate expression is used to combine the effects of these two reactions. A similar approach was implemented by Nicolin $et.\ al.$ in [24] to address the same issue. The reaction rate for (1) is formulated in the form of an Arrhenius equation, and is expressed as:

$$R_T = A_T\ e^{-\frac{E_a^T}{RT}}\ \frac{m_C}{M_C} X_{O_2} \tag{2}$$

The presence of cerium provides additional reaction pathways for carbon. Endothermic reactions occupy active ceria (CeO_2) sites in the catalytic coating, while consuming carbon molecules. This procedure is described by the following chemical reactions [34]:

$$\left.\begin{array}{l} C + 4CeO_2 \rightarrow 2Ce_2O_3 + CO_2 \\ C + 2CeO_2 \rightarrow Ce_2O_3 + CO \end{array}\right\} \textbf{Endothermic} \tag{3}$$

which lead to the lumped reaction kinetics of equation (4):

$$R_{C,1} = A_{C,1}\ e^{-\frac{E_a^{C,1}}{RT}}\ \frac{m_C}{M_C} X_{CeO_2} \tag{4}$$

Combining reaction kinetics for (1) and (3) into (2) and (4), respectively, stiffens the response of the model, but also removes additional uncertain parameters given by the intrinsic competition between the exothermic and endothermic reactions for carbon. In contrast, the exothermic reaction in equation (5) generates new free ceria sites, oxidizing Ce_2O_3 and producing CeO_2 [34]:

$$\left.\begin{array}{l} Ce_2O_3 + 0.5O_2 \rightarrow 2CeO_2 \end{array}\right\} \textbf{Exothermic} \tag{5}$$

which leads to the following reaction kinetics:

$$R_{C,2} = A_{C,2}\ e^{-\frac{E_a^{C,2}}{RT}}\ \frac{X_{O_2}\ \rho_{O_2}\ V_{trap}}{M_{O_2}}(1 - X_{CeO_2}), \tag{6}$$

where ρ_{O_2} is obtained using the ideal gas equation.

Lumping the gas and solid phases together, the thermal dynamics inside the GPF are described as follows:

$$\frac{dT_{mod}}{dt} = \Big[\overbrace{-\Delta H_T R_T - \Delta H_{C,2} R_{C,2}}^{\text{Exothermic}} \overbrace{-\Delta H_{C,1} R_{C,1}}^{\text{Endothermic}} - \dot{m}_g\ C_{p,g}(T_{mod} - T_{inlet})\Big] \frac{1}{V_{GPF}\ \rho_{GPF}\ C_{p,GPF}} \tag{7}$$

where $(-\Delta H_T)R_T$ and $(-\Delta H_{C,2})R_{C,2}$ are the exothermic heat of the reactions (1) and (5) respectively, and $(-\Delta H_{C,1})R_{C,1}$ is the endothermic heat of the reaction (3). The sign convention of equation (7) accounts for exothermic enthalpy of formations being negative and endothermic enthalpy of formations being positive [35].

The enthalpy of formation of a substance, ΔH_f, represents the amount of energy absorbed or released as the substance is formed from its constituent elements [35]. When the control volume is merely composed of these elements, exothermic reactions release chemical energy from the control volume as heat; hence ΔH_f is negative. The converse is true for endothermic reactions. The dynamic equation for the GPF lumped model represents the filter and not the specific elemental molecules. So, heat leaving the molecular scale control volume due to product formation is actually flowing into the GPF material. This necessitates the need for the negative signs in equation (7).

The soot mass oxidation dynamics are modeled under the assumption of uniform deposition and concentration inside the device [24]. Accordingly, the temporal dynamics of

carbon mass within the GPF can be modeled by:

$$\frac{dm_C}{dt} = -A_T\ e^{-\frac{E_a^T}{RT}}\ m_C\ X_{O_2} - A_{C,1}\ e^{-\frac{E_a^{C,1}}{RT}}\ m_C\ X_{CeO_2} \quad (8)$$

Additionally, the formation-consumption of available ceria sites for carbon interaction is modeled by:

$$\frac{dX_{CeO_2}}{dt} = -A_{C,1}\ e^{-\frac{E_a^{C,1}}{RT}}\ \frac{m_C}{\rho_{soot}\ V_{trap}} X_{CeO_2} + A_{C,2}\ e^{-\frac{E_a^{C,2}}{RT}}\ X_{O_2}(1 - X_{CeO_2}) \quad (9)$$

X_{CeO_2} in equation (9) represents the volume fraction of active ceria sites. The volume fraction of a constituent in a medium is generally defined as the ratio of the volume occupied by the constituent to the total volume occupied by all the constituents. The soot oxidation reactions (1) and (4), the soot mass dynamic equation (8), and the mass fraction variation equation of available ceria sites (9), depend on X_{O_2}, the volume fraction of oxygen. Under nominal operating conditions, where the air-fuel ratio, λ, is equal to the stoichiometric value of 1.0, X_{O_2} is equal to zero. This assumes complete gasoline combustion and that the GPF is located downstream of the TWC. During a GPF regeneration event, the engine is forced to operate in lean conditions where λ is greater than 1.0. This increases the concentration of oxygen inside the GPF and consequently enables the reaction pathways (1), (3), and (5). These reaction rates increase with GPF temperature, leading to the accelerated oxidation of the trapped particulate matter. X_{O_2} is computed using the measurements provided by a wide range lambda sensor located upstream of the GPF, and simultaneously involving the following combustion reaction [36]:

$$C_aH_b + \lambda\left(a + \tfrac{b}{4}\right)(O_2 + 3.773N_2) \rightarrow aCO_2 + \tfrac{b}{2}H_2O + \lambda 3.773\left(a + \tfrac{b}{4}\right)N_2 + (\lambda - 1)\left(a + \tfrac{b}{4}\right)O_2 \quad (10)$$

The total number of moles of the products of the above equation, which are also constituents of the exhaust gas, are:

$$n_{tot} = a + \frac{b}{2} + \lambda 3.773\left(a + \frac{b}{4}\right) + (\lambda - 1)\left(a + \frac{b}{4}\right) \quad (11)$$

Considering $C_aH_b = C_8H_{18}$ (octane), the volume fraction of oxygen is determined by the ratio of oxygen moles to the total number of combustion product moles:

$$X_{O_2} = \frac{(\lambda - 1)(a + b/4)}{n_{tot}} \quad (12)$$

III. Parameter Identification Study

In order to identify the lumped parameter model proposed in Section II, experimental measurements of GPF inlet temperature, GPF brick temperature, and exhaust gas mass flow rate are used. The sensor layout for temperature data acquisition is shown in Figure 1. Type K thermocouples were used to measure the GPF inlet (T_{inlet}) and mid-location (T_{mid}) temperatures. Parameter identification is performed by considering regeneration events that occur within the filter. A total of 11 parameters are identified using experimental data, with the vector of parameters, θ, being:

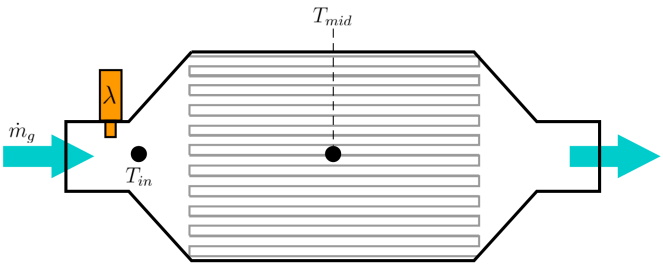

Fig. 1: GPF sensor layout: 2 thermocouples (T_{inlet},T_{mid}) are used to identify the lumped parameter model. Upstream the GPF, a wide-band λ sensor measures the amount of oxygen going into the filter.

$$\theta = [A_T\ A_{C,1}\ A_{C,2}\ E_a^T\ E_a^{C,1}\ E_a^{C,2}\ \Delta H_T\ \Delta H_{C,1}\ \Delta H_{C,2}\ C_{p,GPF}\ C_{p,g}]^T \quad (13)$$

The parameters are identified using the Particle Swarm Optimization (PSO[1]) algorithm [39]. The objective of the parameter identification study is to determine the element values of the vector θ, such that the model output matches the experimental measurement as closely as possible. Mathematically, this is defined using the thermal-based cost function:

$$J(\theta) = \sqrt{\left\{\frac{1}{N}\sum_{i=1}^{N}\left(T_{mid}(i) - T_{mod}(\theta; i)\right)^2\right\}} \cdot \frac{100 \cdot N}{\sum_{i=1}^{N} T_{mid}(i)} \quad (14)$$

where T_{mid} is the measured temperature at the mid-location internally in the GPF, T_{mod} is the model-predicted temperature that is a function of θ, N is the total number of data samples, and i is the time index. The expression for the cost function also represents the % root mean square (RMS) error.

The parameter identification study was conducted using two different experimental data sets that were characterized by different initial soot loading concentrations, typically expressed in units of g/l. In the experimental campaign, a ceria-coated GPF was instrumented with thermocouples that spanned the axial direction from inlet to outlet, and the radial direction from centerline to exterior shell. Among these thermocouples, the mid-location was chosen as a representation of the internal temperature of the GPF. This selection was made due to the strategic location of the thermocouple, coupled with the fact that the lumped parameter model would consider uniform behavior across the entire GPF. As such, the center location would be a characteristic representation of the behavior of the entire GPF device.

[1]PSO is a non-gradient based evolutionary computational approach based on the social behavior of certain animal species [37]. It is designed to achieve the global minumum for a designed objective/fitness function by moving a population of possible solutions, constituting the *swarm*, through a multi-dimensional solution hyperspace in an iterative fashion [38].

TABLE I: The range of variation of the parameter values during the identification process.

Parameter	Identification Range
A_T	$[1e5, 3e8]$
$A_{C,1}$	$[10, 3e4]$
$A_{C,2}$	$[10, 3e4]$
E_a^T	$[135e3, 165e3]$
$E_a^{C,1}$	$[90e3, 110e3]$
$E_a^{C,2}$	$[72e3, 88e3]$
ΔH_T	$[-302.4e3, -226.8e3]$
$\Delta H_{C,1}$	$[255.84e3, 351.78e3]$
$\Delta H_{C,2}$	$[-457.44e3, -343.08e3]$
$C_{p,GPF}$	$[112, 1344]$
$C_{p,g}$	$[100, 1200]$

Prior to data acquisition, soot accumulation experiments were performed by operating a vehicle with the instrumented GPF installed downstream of a TWC for extended periods of time. Specific operating regimes were designed for expedient accumulation of soot within the GPF without elevating exhaust temperatures above the activation threshold of the GPF reactions. Based on engine operating conditions, the exhaust gas mass flow, and the backpressure across the GPF that was measured using a differential pressure sensor, particulate mass accumulation inside the GPF was determined. Several accumulation experiments were conducted to produce different initial soot loading concentrations within the coated-GPF. The identification study presented in this section used two experimental data sets: one with an initial soot loading concentration of $0.5\ g/l$, and the other with an initial soot loading concentration of $2.15\ g/l$.

For each data set, a series of regeneration events were conducted in succession to oxidize the soot (carbon) particulate matter. Successive regeneration events were initiated at increasingly elevated GPF inlet temperatures to facilitate further oxidation of the trapped particulate matter as the GPF soot loading diminished. For the identification study, the first regeneration events conducted on the coated-GPF for initial soot loading concentrations of $0.5\ g/l$ and $2.15\ g/l$ were utilized, as the absolute concentration of soot within the GPF is explicitly known. This is an important input for the lumped parameter model in order to characterize the thermal dynamics. Since these experiments did not involve data acquisition pertaining to the amount of soot oxidized, it is appropriate to select the first regeneration event where the initial amount of soot has been clearly determined from the accumulation experiment.

The elements of the vector θ comprise pre-exponential factors, activation energies, and reaction enthalpies for (1), (3), and (5). The initial guesses for the pre-exponential factors and the activation energies are based on the work on Konstantas [34]. The reaction enthalpies are explicitly calculated for the three reaction pathways using the thermodynamic enthalpies of formation of the reactants and products, the values for which were obtained from [40]. The initial values for cordierite and exhaust gas specific heat capacities were obtained from [41] and [35], respectively.

The parameter identification study was conducted using the PSO algorithm [39], with a population size of 200 and 2,000 total generations. The termination criteria was defined as either 2,000 completed generations (or) the completion of 1,000 successive generations without any improvement in the cost function. Table I lists the range of the identification space for the elements of the parameter vector θ. Specification of such large identification ranges accounts for a loss in the physical meaning of the lumped model parameters due to the inherent assumption of uniform GPF transport dynamics throughout the medium. It must be noted that since the equations presented in (1) and (3) are lumped, the initial values for their corresponding reaction enthalpies, $\Delta H_{C,1}$ and $\Delta H_{C,2}$, are obtained by taking the average of the reaction enthalpy of each individual reaction shown in (1) and (3), respectively. At the sponsor's request, the identified values of the model parameters have remained proprietary.

The results of the parameter identification study using the $0.5\ g/l$ and $2.15\ g/l$ experimental data sets are presented in Figure 2. $Domain\ 1$ represents pre-regeneration temperature dynamics, $Domain\ 2$ represents temperature dynamics during the onset and completion of regeneration, and $Domain\ 3$ represents post-regeneration temperature dynamics. The RMS error for the identification results using the $0.5\ g/l$ and the $2.15\ g/l$ data sets are respectively 1.53% and 1.76%. The next section presents model validation over a third experimental data set and a discussion on the potential implications of the control-oriented model presented in Section II.

IV. Model Validation

The identified parameters from the two different experimental data sets depend on the initial soot loading concentration. In order to validate the model, the experimental data set for the first regeneration event of a coated-GPF with an initial soot loading concentration of $1.0\ g/l$ was chosen. This particular data set was selected because the initial soot mass inside the GPF was between the initial soot mass values for the data sets used for parameter identification. The model parameter values used for validation were obtained by taking the average of the parameter values from the identification results using the $0.5\ g/l$ and $2.15\ g/l$ data sets. The validation results are presented in Figure 3. In addition to the initial soot loading, temperature effects are also predominant across the GPF and influence the model parameters. Current research is investigating the development of a linear parameter-varying (LPV) model, which would incorporate the dependency of both initial soot loading and temperature to provide linearly interpolated values of the model parameters for different operating conditions.

The RMS error for the model validation using the $1.0\ g/l$ data set is 4.03%. The validation results indicate satisfactory accuracy of the model-predicted thermal dynamics with respect to the experimentally observed temperature dynamics in $Domain\ 1$ and $Domain\ 3$. The discrepancy observed in $Domain\ 2$ may be attributed to the limitations of using

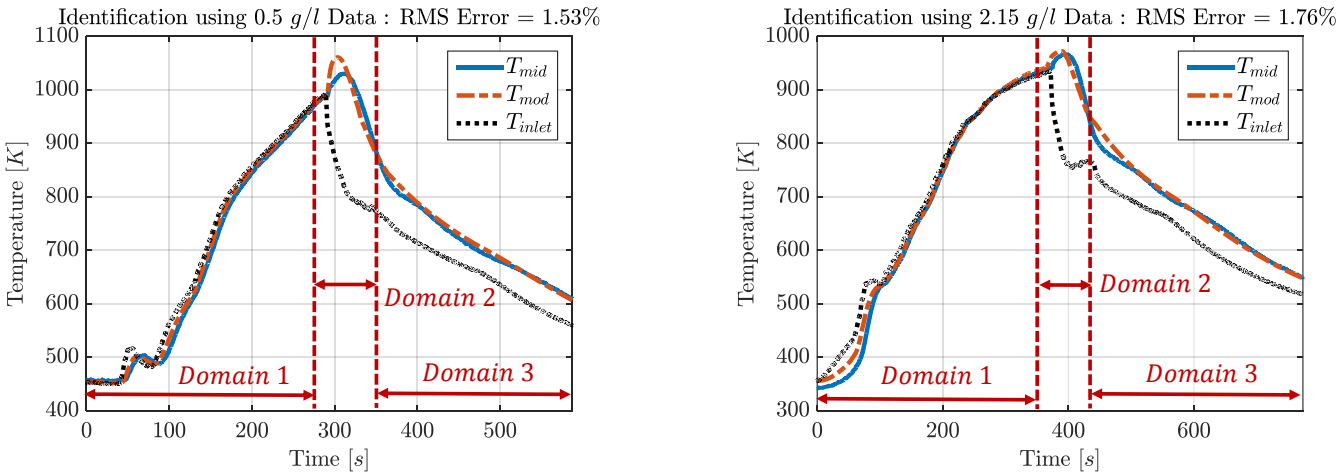

Fig. 2: Results of the parameter identification study comparing the measured and model-predicted GPF mid-location internal temperature variation. The RMS error for the identification results using the $0.5\ g/l$ *and* $2.15\ g/l$ *data sets are respectively* 1.53% *and* 1.76%.

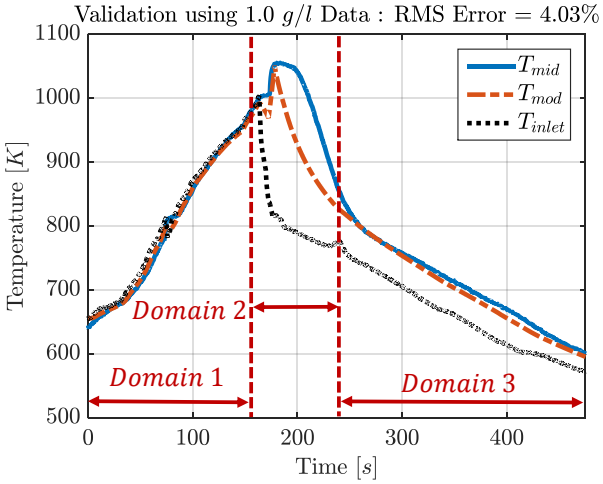

Fig. 3: Model validation results comparing the measured and model-predicted GPF mid-location internal temperature during the first regeneration event of a coated-GPF with an initial soot loading of $1.0\ g/l$. *The RMS error from the validation results of the model is* 4.03%.

a lumped parameter model, which assumes a uniformly even dispersion of soot throughout the filter and a single filter temperature. In reality, the response of mid GPF temperature sensor is impacted by heat emanating from soot reactions in other areas either by transport or by conduction through the cordierite. A lumped parameter model is unable to account for spatial distribution due to its assumption of uniform dynamics throughout the GPF. Despite these discrepancies, the maximum mid-location experimental and model-predicted temperature values based for the $1.0\ g/l$ data set are respectively $1056\ K$ and $1050\ K$. The maximum mid-location temperature predicted by the model was within an error of 0.57% of the measured maximum mid-location temperature.

These validation results have strong implications for two reasons: (a) the model utilizes only the GPF inlet temperature to predict internal thermal dynamics, eliminating the need for expensive and high-maintenance internal GPF temperature sensors during vehicle operation, and (b) the health of the GPF washcoat and cordierite substrate are sensitive to high internal temperatures. Exposing the coated GPF to aggressive conditions may result in performance degradation, as well as material disintegration and failure [24]. To address this critical issue, the model can be used to develop On-Board Diagnostic (OBD) strategies to determine the onset temperature and the duration for which regeneration events must be performed. By successful implementation of such model-based control strategies, critical internal GPF temperatures can be avoided during nominal operation.

V. Conclusions and Future Work

This paper presented a control-oriented model to predict the thermal response of a ceria-coated GPF during nominal operation and regeneration events. The model incorporated oxygen- and ceria-initiated soot oxidation reactions, and both the heat generated inside the coated GPF during regeneration and the heat carried away by the exhaust gases. A thermal-based cost function was developed to identify the model parameters by minimizing the RMS error between the model-predicted GPF thermal response and the experimentally measured temperature at the axial center of the coated GPF.

Parameter identification studies were conducted using experimental data on two different initial soot loading concentrations. The model was validated for a third data set whose initial soot loading concentration was between those used for identification. Results indicate that the model is suitable for predicting internal temperature dynamics for ceria-coated GPFs. Current and future work will focus on the following aspects to enhance model predictability: a) experimental work to quantitatively measure soot oxidation dynamics in addition to thermal data acquisition, b) reducing the number of identified parameters by determining exhaust gas and cordierite properties using experimental data, and c) improving the parameter identification study by incorporating soot oxidation dynamics in the cost function.

ACKNOWLEDGEMENT

The authors gratefully acknowledge the support of our sponsor, Fiat Chrysler Automobiles (FCA) US LLC, for granting permission to utilize experimental data from our research collaboration. Responsibility for the content lies with the authors of this work.

REFERENCES

[1] "Summary of the Clean Air Act." https://www.epa.gov/laws-regulations/summary-clean-air-act. Accessed: 2017-02-25.

[2] A. G. Boulanger, A. C. Chu, S. Maxx, and D. L. Waltz, "Vehicle Electrification: Status and Issues," *Proceedings of the IEEE*, vol. 99, no. 6, pp. 1116–1138, 2011.

[3] B. Guan, R. Zhan, H. Lin, and Z. Huang, "Review of the state-of-the-art of exhaust particulate filter technology in internal combustion engines," *Journal of Environmental Management*, vol. 154, pp. 225–258, 2015.

[4] T. V. Johnson and A. Joshi, "Directions in vehicle efficiency and emissions," *Combustion Engines*, vol. 55, 2016.

[5] H. Wei, T. Zhu, G. Shu, L. Tan, and Y. Wang, "Gasoline engine exhaust gas recirculation - A review," *Applied Energy*, vol. 99, pp. 534–544, 2012.

[6] C. Sprouse and C. Depcik, "Review of organic Rankine cycles for internal combustion engine exhaust waste heat recovery," *Applied Thermal Engineering*, vol. 51, no. 1, pp. 711–722, 2013.

[7] B. Guan, R. Zhan, H. Lin, and Z. Huang, "Review of state of the art technologies of selective catalytic reduction of NO_x from diesel engine exhaust," *Applied Thermal Engineering*, vol. 66, no. 1, pp. 395–414, 2014.

[8] R. Zhu, J. Hu, X. Bao, L. He, Y. Lai, L. Zu, Y. Li, and S. Su, "Tailpipe emissions from gasoline direct injection (GDI) and port fuel injection (PFI) vehicles at both low and high ambient temperatures," *Environmental Pollution*, vol. 216, pp. 223–234, 2016.

[9] J. F. Rodriguez and W. K. Cheng, "Effect of Operation Strategy on First Cycle CO, HC, and PM/PN Emissions in a GDI Engine," *SAE International Journal of Engines 2015-01-0887*, 2015.

[10] P. Karjalainen, L. Pirjola, J. Heikkilä, T. Lähde, T. Tzamkiozis, L. Ntziachristos, J. Keskinen, and T. Rönkkö, "Exhaust particles of modern gasoline vehicles: A laboratory and an on-road study," *Atmospheric Environment*, vol. 97, pp. 262–270, 2014.

[11] T. Johnson, "Vehicular emissions in review," *SAE International Journal of Engines*, vol. 9, no. 2016-01-0919, pp. 1258–1275, 2016.

[12] C. Myung and S. Park, "Exhaust nanoparticle emissions from internal combustion engines: A review," *International Journal of Automotive Technology*, vol. 13, no. 1, pp. 9–22, 2012.

[13] M. M. Maricq, J. J. Szente, J. Adams, P. Tennison, and T. Rumpsa, "Influence of mileage accumulation on the particle mass and number emissions of two gasoline direct injection vehicles," *Environmental Science & Technology*, vol. 47, no. 20, pp. 11890–11896, 2013.

[14] Y. Ito, T. Shimoda, T. Aoki, Y. Shibagaki, K. Yuuki, H. Sakamoto, C. Vogt, T. Matsumoto, W. Heuss, *et al.*, "Advanced ceramic wall flow filter for reduction of particulate number emission of direct injection gasoline engines," *SAE Technical Paper 2013-01-0836*, 2013.

[15] T. W. Chan, M. Saffaripour, F. Liu, J. Hendren, K. A. Thomson, J. Kubsh, R. Brezny, and G. Rideout, "Characterization of real-time particle emissions from a gasoline direct injection vehicle equipped with a catalyzed gasoline particulate filter during filter regeneration," *Emission Control Science and Technology*, vol. 2, pp. 75–88, 2016.

[16] B. Opitz, A. Drochner, H. Vogel, and M. Votsmeier, "An experimental and simulation study on the cold start behaviour of particulate filters with wall integrated three way catalyst," *Applied Catalysis B: Environmental*, vol. 144, pp. 203–215, 2014.

[17] G. Stratakis, D. Psarianos, and A. Stamatelos, "Experimental investigation of the pressure drop in porous ceramic diesel particulate filters," *Proceedings of the Institution of Mechanical Engineers, Part D: Journal of Automobile Engineering*, vol. 216, pp. 773–784, 2002.

[18] S. Yang, C. Deng, Y. Gao, and Y. He, "Diesel particulate filter design simulation: A review," *Advances in Mechanical Engineering*, vol. 8, no. 3, 2016.

[19] G. C. Koltsakis and A. M. Stamatelos, "Modes of catalytic regeneration in diesel particulate filters," *Industrial & Engineering Chemistry Research*, vol. 36, no. 10, pp. 4155–4165, 1997.

[20] S.-J. Lee, S.-J. Jeong, and W.-S. Kim, "Numerical design of the diesel particulate filter for optimum thermal performances during regeneration," *Applied Energy*, vol. 86, no. 7, pp. 1124–1135, 2009.

[21] G. J. Thompson, D. K. Carder, M. C. Besch, A. Thiruvengadam, and H. Kappana, "In-use emissions testing of light-duty diesel vehicles in the united states," *Retrieved from the International Council on Clean Transportation Website*, 2014.

[22] E. A. Kladopoulou, S. L. Yang, J. H. Johnson, G. G. Parker, and A. G. Konstandopoulos, "A study describing the performance of diesel particulate filters during loading and regeneration - A lumped parameter model for control applications," *SAE Technical Paper*, 2003.

[23] M. Kostoglou and A. G. Konstandopoulos, "Effect of soot layer microstructure on diesel particulate filter regeneration," *AIChE Journal*, vol. 51, no. 9, pp. 2534–2546, 2005.

[24] P. Nicolin, D. Rose, F. Kunath, and T. Boger, "Modeling of the soot oxidation in gasoline particulate filters," *SAE Technical Paper 2015-04-14*, 2015.

[25] T. Boger, D. Rose, P. Nicolin, N. Gunasekaran, and T. Glasson, "Oxidation of soot (printex® u) in particulate filters operated on gasoline engines," *Emission Control Science and Technology*, vol. 1, no. 1, pp. 49–63, 2015.

[26] X. Liu, J. Kim, T. Chanko, C. Lambert, and J. Pakko, "A Modeling Analysis of Fibrous Media for Gasoline Particulate Filters," *SAE Technical Paper 2017-01-0967*, 2017.

[27] G. Pozzato, M. A. Hoffman, and S. Onori, "Multi-channel physics-based modeling and experimental validation of an uncoated gasoline particulate filter in clean operating conditions," in *Proceedings of the American Control Conference (ACC)*, pp. 5392–5397, IEEE, 2017.

[28] J. M. Richter, R. Klingmann, S. Spiess, and K.-F. Wong, "Application of catalyzed gasoline particulate filters to GDI vehicles," *SAE International Journal of Engines*, vol. 5, no. 2012-01-1244, 2012.

[29] C. Morgan, "Platinum group metal and washcoat chemistry effects on coated gasoline particulate filter design," *Johnson Matthey Technology Review*, vol. 59, no. 3, pp. 188–192, 2015.

[30] M. Dietrich, C. Jahn, P. Lanzerath, and R. Moos, "Microwave-based oxidation state and soot loading determination on gasoline particulate filters with three-way catalyst coating for homogenously operated gasoline engines," *Sensors*, vol. 15, no. 9, pp. 21971–21988, 2015.

[31] C. Lambert, T. Chanko, D. Dobson, X. Liu, and J. Pakko, "Gasoline Particulate Filter Development," *Emission Control Science and Technology*, vol. 3, no. 1, pp. 105–111, 2017.

[32] S. Inoda, Y. Nomura, H. Ori, and Y. Yabuzaki, "Development of New Coating Technology Optimized for Each Function of Coated GPF," *SAE Technical Paper 2017-01-0929*, 2017.

[33] R. Zhan, S. T. Eakle, and P. Weber, "Simultaneous Reduction of PM, HC, CO, and NO_x Emissions from a GDI Engine," *SAE Technical Paper 2010-01-0365*, 2010.

[34] G. Konstantas and A. Stamatelos, "Computer aided engineering of diesel filter systems," in *Joint Meeting of the Italian and the Greek Section of the Combustion Institute*, pp. 17–19, 2004.

[35] Y. A. Çengel and M. A. Boles, *Thermodynamics: An Engineering Approach*. McGraw-Hill series in Mechanical Engineering, McGraw-Hill Higher Education, 2006.

[36] J. Heywood, *Internal Combustion Engine Fundamentals*. McGraw-Hill Education, 1988.

[37] M. A. Rahman, S. Anwar, and A. Izadian, "Electrochemical model parameter identification of a lithium-ion battery using particle swarm optimization method," *J. Power Sources*, vol. 307, pp. 86–97, 2016.

[38] N. Chakraborti, R. Jayakanth, S. Das, E. D. Çalişir, and Ş. Erkoç, "Evolutionary and Genetic Algorithms applied to Li^+-C System: Calculations Using Differential Evolution and Particle Swarm Algorithm," *Journal of Phase Equilibria and Diffusion*, vol. 28, pp. 140–149, 2007.

[39] S. Ebbesen, P. Kiwitz, and L. Guzzella, "A generic particle swarm optimization matlab function," in *Proceedings of the American Control Conference (ACC)*, pp. 1519–1524, IEEE, 2012.

[40] D. Lide and W. Haynes, *CRC Handbook of Chemistry and Physics: A ready-reference book of chemical and physical data*. Boca Raton, Fla: CRC, 2009.

[41] E. C. Robertson, "Thermal properties of rocks," tech. rep., US Geological Survey,, 1988.